6th Workshop on Numerical Methods in Applied
Science and Engineering (NMASE 07)
Vall de Núria, 9 a 11 de enero de 2007


# NEFEM FOR EULER EQUATIONS

**R. Sevilla, S. Fernández-Méndez and A. Huerta**

Laboratori de Càlcul Numèric (LaCàN)
Departament de Matemàtica Aplicada III
Universitat Politècnica de Catalunya
e-mail: {ruben.sevilla, sonia.fernandez, antonio.huerta}@upc.edu
web: http://www-lacan.upc.edu

**Key words:** NURBS, Finite Elements, CAD, Discontinuous Galerkin, exact geometry representation, high-order isoparametric finite elements, compressible flow, Euler equations

**Abstract.** *An improvement of the classical finite element method is proposed in [1], the NURBS-Enhanced Finite Element Method (NEFEM). It considers an exact representation of the geometry by means of the usual CAD description of the boundary with Non-Uniform Rational B-Splines (NURBS). For elements not intersecting the boundary, a standard finite element interpolation and numerical integration is used. Specifically designed piecewise polynomial interpolation and numerical integration are proposed for those finite elements intersecting the NURBS boundary.*

*In [2] a numerical example involving an electromagnetic scattering application, is used in order to demonstrate the applicability and behavior of the proposed methodology. The results are encouraging and show that the NEFEM is more accurate than the corresponding isoparametric finite elements, using a Discontinuous Galerkin (DG) formulation. Recent studies also demonstrate that, for a desired precision, the NEFEM is also more efficient in terms of number of degrees of freedom, and in terms of CPU time.*

*In the present work the NEFEM is reviewed and applied to the solution of the Euler equations of a compressible inviscid fluid. This set of hyperbolic equations represents a more challenging application for the NEFEM because the nonlinearity of the hyperbolic system and the sensitivity of DG formulations to the imposition of the wall boundary condition in curved domains.*

## 1 Introduction

The relevance of an accurate representation of the domain and its boundary has recently been pointed out by several authors, see [3, 4, 5, 6, 7, 8] among others. In some applications, such as compressible flow problems, an important loss of accuracy is observed when a linear approximation of the boundary is used, see [3, 4]. Reference [3]

shows that, in the presence of curved boundaries, a meaningful high-order accurate solution can be obtained only if a corresponding high-order approximation of the geometry is employed (i.e. isoparametric finite elements). A detailed analysis of this problem is performed in [7]. In this work, it is shown that for a consistent boundary discretization in a discontinuous Galerkin finite element method, it is necessary to take into account the effect of the domain boundary curvature. In [8] the same problem is studied, and a new method is proposed for computing the flux across a curved face. Using a parameterization of the curved boundary the flux definition is modified but the resulting method is, unfortunately, non-conservative. Several studies can be found in the literature following these ideas, see for instance [9].

However, the need of an accurate representation of the geometry is not an exclusive matter of fluid mechanics. For instance, similar conclusions are derived in [5] for linear elasticity problems: sizable errors are present in the numerical solution when the order for the geometric approximation is lower than the order of functional interpolation, even for geometries as simple as an sphere. Isoparametric finite elements or superparametric finite elements (i.e. greater order for the geometry) are necessary in order to ensure an accurate enough representation of the geometry. On the other hand, reference [6] analyzes the error induced by the approximation of curvilinear geometries with isoparametric elements. The 3D Maxwell equations are solved in a sphere with isoparametric finite elements and with an exact mapping of the geometry. The exact mapping provides more accurate results, with errors differing by an order in magnitud. Thus, in some applications, an isoparametric representation of the geometry is far from providing an optimal numerical solution for a given finite element discretization.

Recently, [10] proposes a new methodology: the *isogeometric analysis*. Its goal is to consider an exact representation of the geometry, with no dependency on the spatial discretization. In the *isogeometric analysis* the solution of the boundary value problem is approximated with the same NURBS (*Non-Uniform Rational B-Splines*, [11]) base used for the description of the geometry. This idea was first introduced in [12] in the context of thin shell analysis.

The methodology proposed in [1, 2] and reviewed here, the *NURBS-Enhanced Finite Element Method* (NEFEM), follows the same rationale, but it is more simple because of two main differences: *(i)* NEFEM also considers the exact NURBS description for the computational domain, but NURBS are restricted to the boundary of the computational domain, which is the one that usually is directly related to a CAD, and *(ii)* the solution is approximated with standard finite element (FE) polynomial interpolation. Thus, in the large majority of the domain, for elements not intersecting the NURBS boundary, a standard FE interpolation and numerical integration is used, preserving the computational efficiency of classical FE techniques. Specifically designed piecewise polynomial interpolation and numerical integration are proposed for those finite elements intersecting the NURBS boundary.

The use of a piecewise polynomial approximation represents an important advantage

in front of the NURBS functional approximation used in the *isogeometric analysis*: the NEFEM ensures the local reproducibility of polynomials and, therefore, it preserves the classical FE convergence properties.

First, in section 2, a brief NURBS introduction is given. Section 3 reviews the basic concepts and fundamentals of the NEFEM. Special attention is paid to the interpolation and numerical integration in those elements affected by the NURBS description of the boundary. In order to facilitate the explanation, the NEFEM is presented for 2D domains. Although more attention is required to geometrical aspects, the generalization to 3D domains is straightforward. In section 4 the NEFEM is combined with a DG formulation for the numerical solution of the Euler equations. Finally in section 5 the conclusions of this work are presented.

## 2 Basic concepts on NURBS

This section is not devoted to develop or discuss NURBS in detail. There are well known references with excellent presentations of NURBS, see for instance [11]. Here some basic notions are recalled in order to introduce the notation and the concepts employed in following sections.

A $q$th-degree NURBS curve is a piecewise rational function defined in parametric form as

$$\boldsymbol{C}(\lambda) = \frac{\displaystyle\sum_{i=0}^{n_{CP}} C_{i,q}(\lambda)\nu_i \boldsymbol{B}_i}{\displaystyle\sum_{i=0}^{n_{CP}} C_{i,q}(\lambda)\nu_i} \qquad \lambda \in [\lambda_a, \lambda_b], \tag{1}$$

where $\boldsymbol{B}_i$ are the *control points* (determining the *control polygon*), $\nu_i$ are their control weights, the interval $[\lambda_a, \lambda_b]$ is called the *parametric space*, and $C_{i,q}(\lambda)$ are $q$th-degree B-spline basis functions. The B-spline basis functions are defined recursively from the so-called *knot vector* $\Lambda = \{\lambda_0, \dots \lambda_{n_K}\} = \{\underbrace{\lambda_a, \dots, \lambda_a}_{q+1}, \lambda_{q+1}, \dots, \lambda_{n_K-q-1}, \underbrace{\lambda_b, \dots, \lambda_b}_{q+1}\}$ by

$$C_{i,0}(\lambda) = \begin{cases} 1 & \lambda \in [\lambda_i, \lambda_{i+1}) \\ 0 & \lambda \notin [\lambda_i, \lambda_{i+1}) \end{cases} \tag{2}$$

$$C_{i,k}(\lambda) = \frac{\lambda - \lambda_i}{\lambda_{i+k} - \lambda_i} C_{i,k-1}(\lambda) + \frac{\lambda_{i+k+1} - \lambda}{\lambda_{i+k+1} - \lambda_{i+1}} C_{i+1,k-1}(\lambda) \quad \text{for } k = 1 \dots q. \tag{3}$$

Note that the first and final knots must coincide with the endpoints of the parametrization interval and their multiplicity is always $q + 1$. The multiplicity of the remaining knots determines the continuity of the curve at the so-called *breakpoints*, which are no more than the knots without multiplicity. Thus, a NURBS is a piecewise rational function whose definition changes at the breakpoints.

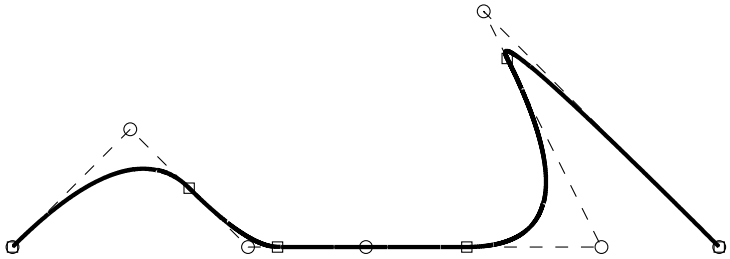

Figure 1: NURBS curve (solid line), control points (∘), control polygon (dashed line) and image of the breakpoints (□)

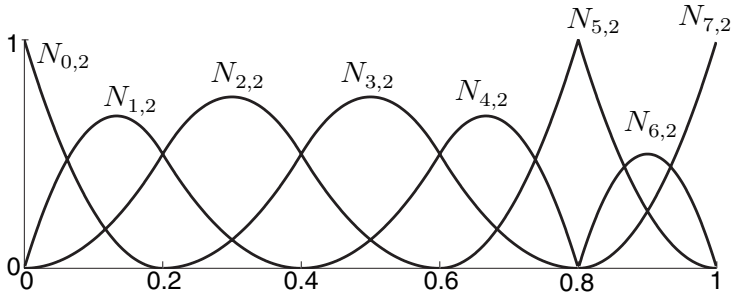


Figure 2: B-spline basis functions for the knot vector $\Lambda = \{0, 0, 0, 0.2, 0.4, 0.6, 0.8, 0.8, 1, 1, 1\}$.

Figure 1 shows a NURBS curve and its control polygon. The corresponding B-spline basis functions are depicted in Figure 2.

A *trimmed* NURBS is defined as the initial parametrization restricted to a subspace of the parametric space. Figure 3 shows the NURBS curve shown in Figure 1 trimmed to the subinterval $[0.05, 0.75]$.

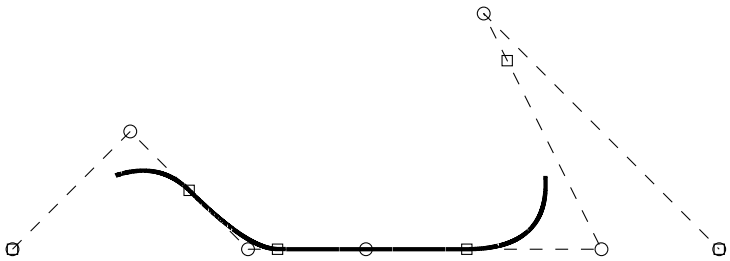

Figure 3: Trimmed NURBS curve for $\lambda \in [0.05, 0.75]$

## 3 NURBS-Enhanced Finite Element Method (NEFEM)

A domain $\Omega \subset \mathbb{R}^2$ is considered, whose boundary $\partial\Omega$, or a portion of its boundary, is defined by NURBS curves [11]. Every NURBS is assumed to be parameterized by

$$\boldsymbol{C} : [\lambda_a, \lambda_b] \longrightarrow \boldsymbol{N}([\lambda_a, \lambda_b]) \subseteq \partial\Omega \subset \mathbb{R}^2.$$

A triangularization of the domain $\overline{\Omega} = \bigcup_e \overline{\Omega_e}$ is also assumed, such that every triangle $\Omega_e$ has at most one side on the NURBS boundary. Figure 4 shows a domain with part of the boundary described by a NURBS circular curve and a valid triangulation for the NEFEM.


Figure 4: Physical domain with part of the boundary defined by a circular NURBS curve (left) and a valid triangulation for the NEFEM (right)

At all elements whose boundary does not intersect the NURBS boundary, the usual FE interpolation and numerical integration is considered. Thus, this section is devoted to the definition of the interpolation and numerical integration at an element with one side on the NURBS boundary.

Let us consider an element $\Omega_e$ with two straight interior sides and one side defined by a trimmed NURBS,

$$\Gamma_e = \boldsymbol{C}([\lambda_1^e, \lambda_2^e]).$$

with $\lambda_a \leq u_1^e < u_2^e \leq \lambda_b$.There are no restrictions in the location of the nodes in the NURBS boundary. The NURBS parametrization can change its definition inside one edge. That is, it is possible to have a *breakpoint* [11] on $(u_1^e, u_2^e)$. This is another advantage with respect to the isogeometric analysis [10].

For each element $\Omega_e$, a triangle $T_e$ is defined using its vertices, see figure 5.

Then, a linear transformation $\boldsymbol{\Psi} : I \longrightarrow T_e$ from the reference triangle $I$ to the straight-sided triangle $T_e$, defined by the vertices of $\Omega_e$, is considered, see Figure 6.

Note that the inverse of this linear transformation maps the triangle $T_e$ into the reference triangle $I$, but also maps the physic element $\Omega_e$ into a curved element in local coordinates with two straight sides, namely

$$I_e := \boldsymbol{\Psi}^{-1}(\Omega_e), \tag{4}$$

see Figure 7.

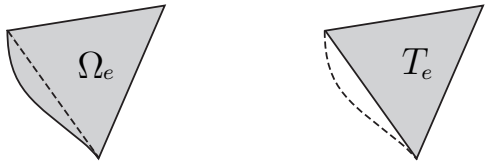


Figure 5: Physic element $\Omega_e$ (left) and triangle $T_e$ defined using its vertices (right)

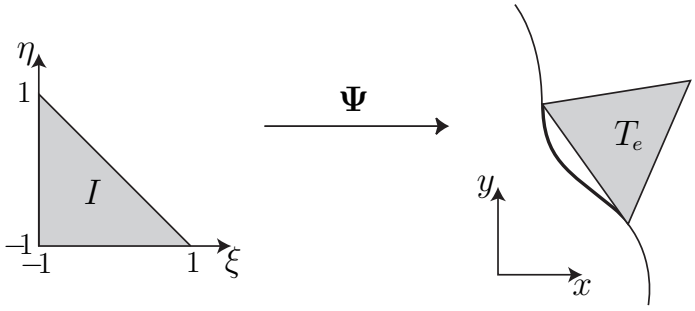


Figure 6: Mapping $\boldsymbol{\Psi}$ defined as the linear transformation from the reference element $I$ to the straight-sided triangle $T_e$ (given by the vertices of $\Omega_e$)

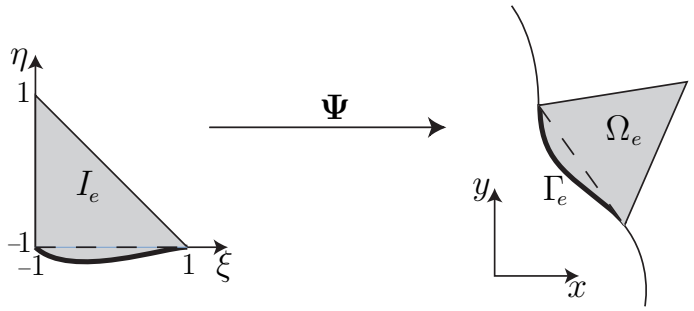


Figure 7: Linear transformation mapping the curved parametric element $I_e := \boldsymbol{\Psi}^{-1}(\Omega_e)$ to the physic element $\Omega_e$

**Remark 1** *Note that the reference element $I$ is the same for all elements $\Omega_e$. However, the curved element $I_e$ depends on the trimmed NURBS defining the curved side $\Gamma_e$ of $\Omega_e$, and therefore it is different for every element $\Omega_e$ intersecting the NURBS boundary.*

**Remark 2** *The use of a linear transformation from the local coordinates $\boldsymbol{\xi}$ in $I_e$ to the cartesian coordinates $\boldsymbol{x}$ in $\Omega^e$, ensures that a polynomial interpolation of degree $m$ in $\boldsymbol{\xi}$ leads to a polynomial interpolation with the same degree in $\boldsymbol{x}$. Thus, the consistency and accuracy of the approximation is ensured even for elements $\Omega_e$ far from being a straight-sided element.*

**Remark 3** *In order to reduce the casuistic in the numerical integration, see section 3.1, it is assumed that the interior vertex of $T_e$ is mapped to the vertex $(-1, 1)$ in $I$. The implementation of this condition only requires a proper local numbering of the vertices of the element.*

Under these assumptions, the FE interpolation base and numerical integration to be used are proposed next.

### 3.1 FE polynomial base

The usual nodal interpolation defined by the Lagrange polynomials is considered in $I_e$, or equivalently, in $\Omega_e$. In order to systematize the computation of the Lagrange polynomials, $\{L_i(\boldsymbol{\xi})\}_{i=1}^{n_{nodes}}$, for any order and for any distribution of nodes, the implementation proposed in [13] is adopted. An orthogonal polynomial base $\{p_i\}_{i=1}^{n_{nodes}}$ is considered in $I_e$, with no dependency on the nodal coordinates $\{\boldsymbol{\xi}_i\}_{i=1}^{n_{nodes}}$. The Lagrange polynomial base is then obtained as

$$L_i = \sum_{j=1}^{n_{nodes}} \left[\boldsymbol{V}^{-1}\right]_{ji} p_j, \tag{5}$$

with the Vandermonde matrix $V_{ij} := p_j(\boldsymbol{\xi}_i)$, for $i, j = 1, \dots, n_{nodes}$.

**Remark 4** *Note that any polynomial base $\{p_i\}$, with no dependency on the nodal coordinates, can be considered for the computation of the Lagrange polynomials using* (5)*. However, an orthogonal polynomial base $\{p_i\}_{i=1}^{n_{nodes}}$, such as the one derived from the well known Jacoby polynomials [13, 14, 15, 16], is advisable in order to ensure a moderate condition number for the Vandermonde matrix $\boldsymbol{V}$. This base also allows an analytical computation of some inner products.*

From an implementation point of view, it is worth noting that all elemental matrices can be first computed for the orthogonal polynomial base, and then transformed with the Vandermonde matrix. That is, let $\boldsymbol{M}_e^p$ be an elemental matrix computed in terms of the orthogonal polynomial base, then $\boldsymbol{M}_e = \boldsymbol{V}^{-T}\boldsymbol{M}_e^p\boldsymbol{V}^{-1}$ is the corresponding elemental matrix for the Lagrange nodal base.

This paper considers equally-spaced distributions of nodes in $I_e$, see left distribution in Figure 8. It corresponds to the usual nodal distribution for the straight-sided reference triangle $I$. Other nodal distributions can also be used. For instance, the right distribution in Figure 8 is adapted in order to locate nodes along the NURBS side. This option makes sense if one wants to set nodal values along the boundary, but it does not represent any advantage if boundary conditions are imposed in weak form, as usual in Discontinuous Galerkin formulations. Moreover, in this case nodal coordinates depend on the curved triangle $I_e$ reducing the computational efficiency of the approach, and leading to a different Vandermonde matrix for each curved element. The use of a nodal distribution with no dependency on the curved element $I_e$, such as the left distribution, is more efficient

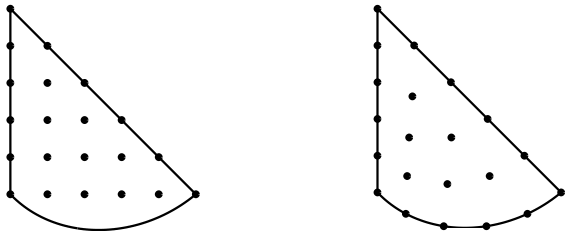

Figure 8: 5th-order nodal distributions in $I_e$: for equally-spaced nodes (left) and adapted to the NURBS side (right)

because of the unique definition of the nodal coordinates and the unique computation of the Vandermonde matrix, with no dependency of the curved element.

It is worth noting that for high-order interpolation ($\geq$ 5-th order) it can be more convenient to use special distributions of nodes in order to reduce the condition number of the resulting elemental matrices, see [17, 18] for details.

### 3.2 Numerical integration

The NEFEM requires the computation of the integral of any function $f$ over an edge given by a trimmed NURBS $\Gamma_e = \boldsymbol{C}([\lambda_1^e, \lambda_2^e])$, that is

$$\int_{\Gamma_e} f \, d\ell = \int_{\lambda_1^e}^{\lambda_2^e} f(\boldsymbol{C}(\lambda)) |J_{\boldsymbol{C}}(\lambda)| \, d\lambda,$$

where $|J_{\boldsymbol{C}}|$ denotes the norm of the differential of the NURBS parameterization $\boldsymbol{C}$. As usual, a 1D numerical quadrature is used for the numerical computation of the integral

$$\int_{\Gamma_e} f \, d\ell \approx \sum_{i=1}^{n} f(\boldsymbol{C}(\lambda_i)) |J_{\boldsymbol{C}}(\lambda_i)| \, \omega_i, \tag{6}$$

where $\lambda_i$ and $\omega_i$ are the coordinates and weights of the $n$ integration points in $[\lambda_1^e, \lambda_2^e]$.

Recall that the parametrization of a trimmed NURBS, $\boldsymbol{C}$, is a piecewise rational function whose definition changes at the breakpoints. Thus, an independent numerical quadrature must be considered for each one of the intervals between breakpoints in order to take into account the discontinuous nature of the parametrization. Numerical experiments reveal that Gauss-Legendre quadratures are a competitive choice in front of other quadrature rules. Numerical experiments also reveal that more popular composite rules, such as the trapezoidal and Simpson composite rules are not suitable for the integration of polynomials along NURBS curves, due to the excessive computational cost.

The NEFEM also requires the computation of integrals over an element $\Omega_e$ with one side $\Gamma_e$ on the NURBS boundary (see Figure 7), that is

$$\int_{\Omega_e} f \, dx \, dy = |J_{\boldsymbol{\Psi}}| \int_{I_e} f \, d\xi \, d\eta \tag{7}$$

where $|J_{\boldsymbol{\Psi}}|$ is the determinant of the Jacobian of the linear transformation $\boldsymbol{\Psi}$, see section 3. The computation of (7) requires the definition of a numerical quadrature for every curved element $I_e$. Two strategies has been studied. The first one is based on a transformation from the straight-edged triangle $\widehat{I}$ given by the vertices $\{(0,0),(1,0),(0,1)\}$, where well-known efficient triangle quadratures can be considered. The second one considers a transformation from a rectangle to the curved element $I_e$. Both transformations are defined under the assumption in Remark 3.

Comparison between these two strategies reveals that the best alternative corresponds to the definition of a transformation from the rectangle $[\lambda_1^e,\lambda_2^e]\times[0,1]$ to the curved element $I_e$, see Figure 9. That is, $\boldsymbol{\varphi}=(\varphi_1,\varphi_2):[\lambda_1^e,\lambda_2^e]\times[0,1]\to I_e$, is given by

$$\varphi_1(\lambda,\zeta):=\phi_1(\lambda)(1-\zeta)-\zeta,\qquad \varphi_2(\lambda,\zeta):=\phi_2(\lambda)(1-\zeta)+\zeta \tag{8}$$

see Figure 9. Using this transformation, integral (7) is computed as

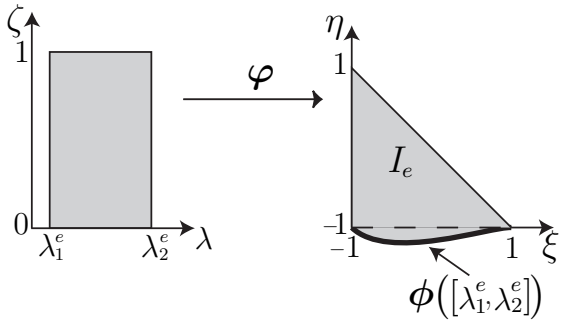


Figure 9: Transformation from $[u_1^e,u_2^e]\times[-1,1]$ to $I_e$ and $\Omega_e$

$$\int_{\Omega_e} f\,dx\,dy=|J_{\boldsymbol{\Psi}}|\int_{I_e} f\,d\xi\,d\eta\simeq|J_{\boldsymbol{\Psi}}|\sum_{i=1}^{n_u}\sum_{j=1}^{n_v} f(\boldsymbol{\xi}_{ij})|J_{\boldsymbol{\varphi}}(\lambda_i,\zeta_j)|\,\omega_i\varpi_j \tag{9}$$

where $\boldsymbol{\xi}_{ij}=\boldsymbol{\varphi}(\lambda_i,\zeta_j)$, $\{\lambda_i,\omega_i\}$ and $\{\zeta_i,\varpi_i\}$ are the 1D quadrature points and weights for the intervals $[\lambda_1^e,\lambda_2^e]$ and $[0,1]$ respectively, and $|J_{\boldsymbol{\varphi}}|$ is the determinant of the Jacobian of the transformation $\boldsymbol{\varphi}$.

**Remark 5** *When the transformation from the rectangle $\boldsymbol{\varphi}$ is considered, the integrals involved in the elemental matrices, for a NEFEM solution with interpolation of degree $p$, can be exactly computed for one of the parameters, $\zeta$, using a Gauss-Legendre quadrature with $p+1$ integration points. The numerical integration for the other direction, given by the NURBS parameter $\lambda$, presents the same difficulty as the integration over a NURBS curve. Moreover, if the geometry is described with a $q$-th degree B-spline, the elemental matrices can be exactly computed with Gauss-Legendre quadratures with $p+1$ integration points for the $\zeta$ parameter, and $q(p+1)$ integration points for the NURBS parameter $\lambda$.*

In the standard FE framework, it is usually preferable to implement a numerical quadrature specifically designed for triangles, see [19]. However, this is not the case for the numerical integration in the NEFEM, where the transformation from the rectangle (8) turns out to be very efficient. For example, Figure 10 shows the integration points, for the computation of the integral $\int_{\Omega_e} x^{10}\, d\Omega$ with an error of about 0.5%, using the transformation depicted in Figure 9 (left with 30 integration points) and using a classical triangle quadrature (right with 54 integration points).

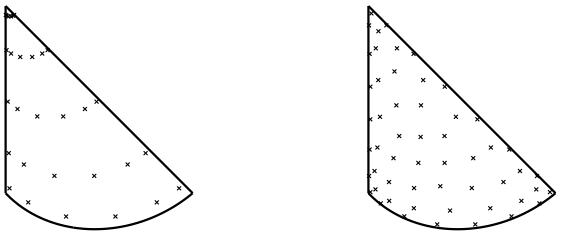

Figure 10: Two numerical quadratures in a curved element

## 4 NUMERICAL EXAMPLE

Euler's equations describes three important conservation laws: (1) conservation of mass, (2) conservation of the momentum, and (3) conservation of total energy. The 2D Euler equations of an inviscid compressible fluid in the absence of external forces, can be written in dimensionless conservative form as

$$\frac{\partial \boldsymbol{U}}{\partial t} + \frac{\partial \boldsymbol{F}_k(\boldsymbol{U})}{\partial x_k} = \boldsymbol{0} \qquad \text{in } \Omega, \tag{10}$$

with

$$\boldsymbol{U} = \begin{pmatrix} \rho \\ \rho v_1 \\ \rho v_2 \\ \rho E \end{pmatrix}, \quad \boldsymbol{F}_1 = \begin{pmatrix} \rho v_1 \\ \rho v_1^2 + p \\ \rho v_1 v_2 \\ (\rho E + p) v_1 \end{pmatrix}, \quad \boldsymbol{F}_2 = \begin{pmatrix} \rho v_2 \\ \rho v_1 v_2 \\ \rho v_2^2 + p \\ (\rho E + p) v_2 \end{pmatrix},$$

where $\rho$ is the density, $\boldsymbol{v} = (v_1, v_2)$ the velocity, $E$ the total energy per unit mass and $p$ is the pressure. This set of nonlinear hyperbolic equations is completed with an equation of state. For a perfect gas, the equation of state is

$$p = (\gamma - 1)\rho\Big(E - \frac{1}{2}\|\boldsymbol{v}\|^2\Big),$$

where $\gamma$ is the polytropic gas constant. The speed of sound is also common in this formulation. It enters in the definition of the Mach number

$$M = \frac{\|\boldsymbol{v}\|}{c},$$

and it is given by

$$c = \sqrt{\frac{\gamma p}{\rho}},$$

see [20, 21] for a detailed presentation.

### 4.1 Subsonic flow around a circle

The numerical test considered is the subsonic flow around a circle at Mach number $M_\infty = 0.3$. Using a DG formulation in [3, 4, 7, 8] it is shown that it is not possible to converge to the steady state solution using linear isoparametric finite elements. Figure 11 show that using the NEFEM it is possible to converge to the steady state solution using linear elements, while the non-physical entropy production behind the wall causes the no convergence of the DG solution.

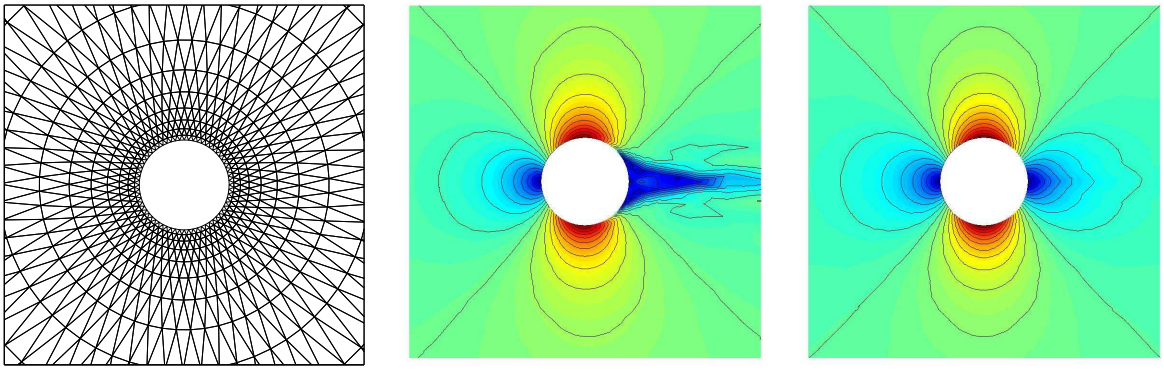

Figure 11: Computational mesh (left), DG solution (center) and NEFEM solution (right) with $p = 1$

Even if the mesh is refined, DG method doesn't achieve the steady state while NEFEM converges to a symmetric solution. NEFEM solution is represented in figure 12.

In the numerical solution of nonlinear hyperbolic problems, such as the Euler equations, it is very usual to work with a nodal interpolation of the fluxes. This options leads to a more efficient computational algorithm but it can be the cause of an instability in the presence of stagnation points, see [22] for more details. To avoid this problem it is necessary to use the so called full quadrature version of the DG method.

## 5 Concluding remarks

In this paper an improvement of the classical finite element method has been proposed for a standard continuous formulation and also for a Discontinuous Galerkin formulation. It considers the exact geometric model by means of the CAD description of the boundary of the domain using Non-Uniform Rational B-Splines. Then, for elements intersecting

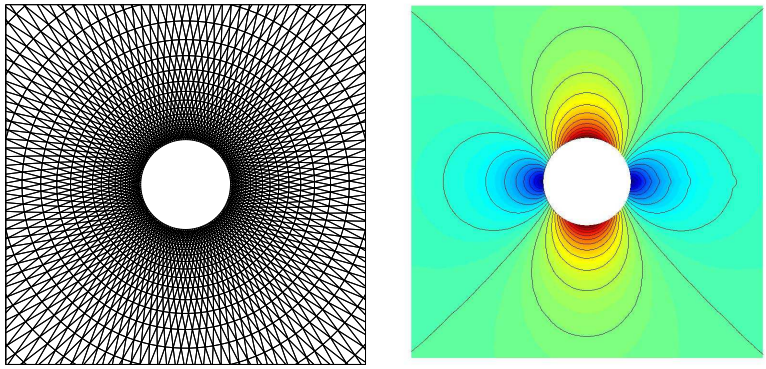

Figure 12: Computational mesh and NEFEM solution with $p = 1$

the boundary a specifically designed polynomial interpolation and numerical integration is proposed.

Preliminar results show the possibilities of the NEFEM approach using low order interpolations. More precisely, numerical examples reveal that using NEFEM the steady state solution of the subsonic flow past a circle problem can be achieved using linear interpolation.

Future work will be focused in the implementation of the full quadrature version of the DG method and the NEFEM solution of the Euler equations using high order interpolations.

## REFERENCES

[1] R. Sevilla, S. Fernández-Méndez, A. Huerta, Nurbs-enhanced finite element method, in: 4rth Workshop on Numerical Methods in Applied Science and Engineering, 2005.

[2] R. Sevilla, S. Fernández-Méndez, A. Huerta, Nurbs-enhanced finite element method for electromagnetic scattering problems, in: 5th Workshop on Numerical Methods in Applied Science and Engineering, 2006.

[3] F. Bassi, S. Rebay, High-order accurate discontinuous finite element solution of the 2D Euler equations, J. Comput. Phys. 138 (2) (1997) 251–285.

[4] T. Barth, Simplified numerical methods for gas dynamics systems on triangulated domains, Ph.D. thesis, Department of Aeronautics and Astronautics, Stanford University (1998).

[5] M. X.J.Luo, J.F.Remacle, Influence of geometric approximation on the accuracy of higher order methods, SCOREC report 1.

[6] D. Xue, L. Demkowicz, Control of geometry induced error in hp finite element (FE) simulations. I. Evaluation of FE error for curvilinear geometries, Int. J. Numer. Anal. Model. 2 (2005) 283–300.

[7] J. Van der Vegt, H. Van der Ven, Discontinuous galerkin discretizations of the euler equations of gas dynamics, in: H. A. Mang, F. G. Rammerstorfer, J. Eberhardsteiner (Eds.), Proceedings of the Fifth World Congress on Computational Mechanics (WCCM V), Vienna University of Technology, 2002.

[8] L. Krivodonova, M. Berger, High-order accurate implementation of solid wall boundary conditions in curved geometries, J. Comput. Phys. 211 (2) (2006) 492–512.

[9] H. Luo, J. D. Baum, R. Löhner, A fast, p-multigrid Discontinuous Galerkin method forcompressible flows at all speeds, in: Proceedings of the 44th AIAA Aerospace Sciences Meeting and Exhibit, AIAA, Reno, Nevada, 2006.

[10] T.J.R. Hughes, J.A. Cottrell, Y. Bazilevs, Isogeometric analysis: CAD, finite elements, NURBS, exact geometry and mesh refinement, Comput. Methods Appl. Mech. Eng. 194 (39–41) (2005) 4135–4195.

[11] L. Piegl, W. Tiller, The NURBS Book, Springer-Verlag, London, 1995.

[12] F. Cirak, M. Ortiz, P. Schröder, Subdivision surfaces: A new paradigm for thin-shell finite-element analysis, Int. J. Numer. Meth. Engrg. 47 (12) (2000) 2039–2072.

[13] J. S. Hesthaven, T. Warburton, Nodal high-order methods on unstructured grids. I. Time-domain solution of maxwell's equations, J. Comput. Phys. 181 (1) (2002) 186–221.

[14] G. E. Karniadakis, S. J. Sherwin, Spectral/hp Element methods for CFD, Numerical Mathematics and Scientific computation, Oxford University Press, 1999.

[15] G. Szegö, Orthogonal Polynomials (fourth edition), Americam Mathematical Society, Providence, 1975.

[16] M. Dubiner, Spectral methods on triangles and other domains, J. Sci. Comput. 6 (1991) 345–390.

[17] Q. Chen, I. Babuška, Approximate optimal points for polynomial interpolation of real functions in an interval and in a triangle, Comput. Methods Appl. Mech. Eng. 128 (3–4) (1995) 405–417.

[18] Q. Chen, I. Babuška, The optimal symmetrical points for polynomial interpolation of real functions in the tetrahedron, Comput. Methods Appl. Mech. Eng. 137 (1996) 89–94.

[19] S. Wandzura, H. Xiao, Symmetric quadrature rules on a triangle, Comput. Math. Appl. 45 (12) (2003) 1829–1840.

[20] C. Hirsch, Numerical Computation of Internal and External Flows. Volume 1: Fundamentals of Numerical Discretization., John Wiley & Sons, 1988.

[21] J. Donea, A. Huerta, Finite Element Methods for Flow Problems, J. Wiley & Sons, 2002.

[22] P. G. Koen Hillewaert, Nicolas Chevaugeon, J.-F. Remacle, Hierarchic multigrid iteration strategy for the discontinuous galerkin solution of the steady euler equations, Internat. J. Numer. Methods Fluids 51 (2006) 1157–1176.

Con el apoyo de *Generalitat de Catalunya* y *Universitat Politècnica de Catalunya*